BBA - Biomembranes 1860 (2018) 1216–1230

Contents lists available at ScienceDirect

BBA - Biomembranes

journal homepage: www.elsevier.com/locate/bbamem

Insertion of Dengue E into lipid bilayers studied by neutron reflectivity and molecular dynamics simulations

Juan M. Vanegas[a,1,2], Frank Heinrich[b,c,2], David M. Rogers[a,3], Bryan D. Carson[a], Sadie La Bauve[a], Briana C. Vernon[a], Bulent Akgun[b,4], Sushil Satija[b], Aihua Zheng[d,5], Margaret Kielian[d], Susan B. Rempe[a], Michael S. Kent[a,*]

[a] Sandia National Laboratories, Albuquerque, NM, United States
[b] National Institute of Standards and Technology Center for Neutron Research, Gaithersburg, MD, United States
[c] Department of Physics, Carnegie Mellon University, Pittsburgh, PA, United States
[d] Department of Cell Biology, Albert Einstein College of Medicine, Bronx, NY, United States

ARTICLE INFO

Keywords:
Dengue virus
Membrane fusion
Envelope protein
Fundamental interactions
Neutron reflectivity
Molecular dynamics simulations

ABSTRACT

The envelope (E) protein of Dengue virus rearranges to a trimeric hairpin to mediate fusion of the viral and target membranes, which is essential for infectivity. Insertion of E into the target membrane serves to anchor E and possibly also to disrupt local order within the membrane. Both aspects are likely to be affected by the depth of insertion, orientation of the trimer with respect to the membrane normal, and the interactions that form between trimer and membrane. In the present work, we resolved the depth of insertion, the tilt angle, and the fundamental interactions for the soluble portion of Dengue E trimers (sE) associated with planar lipid bilayer membranes of various combinations of 1-palmitoyl-2-oleoyl-*sn*-glycero-3-phosphocholine (POPC), 1-palmitoyl-2-oleoyl-*sn*-glycero-3-phospho-rac-glycerol (POPG), 1-palmitoyl-2-oleoyl-*sn*-glycero-3-phosphoethanolamine (POPE), and cholesterol (CHOL) by neutron reflectivity (NR) and by molecular dynamics (MD) simulations. The results show that the tip of E containing the fusion loop (FL) is located at the interface of the headgroups and acyl chains of the outer leaflet of the lipid bilayers, in good agreement with prior predictions. The results also indicate that E tilts with respect to the membrane normal upon insertion, promoted by either the anionic lipid POPG or CHOL. The simulations show that tilting of the protein correlates with hydrogen bond formation between lysines and arginines located on the sides of the trimer close to the tip (K246, K247, and R73) and nearby lipid headgroups. These hydrogen bonds provide a major contribution to the membrane anchoring and may help to destabilize the target membrane.

1. Introduction

All enveloped viruses have a dedicated protein that promotes fusion between viral and host membranes [1–3]. Fusion proteins are critical for infectivity and are targets of therapeutic intervention. All fusion proteins have a hydrophobic peptide sequence that inserts into the host membrane although the sequences and structures vary considerably among the different enveloped viruses. Although many structures have been solved, the functional mechanisms of fusion proteins and their hydrophobic peptides are still under considerable debate [4,5]. Possible functions include anchoring into the host membrane strongly enough to support the high-energy membrane bending that must occur to form a fusion stalk; [4,6–8] promoting positive curvature in the target membrane and dimple formation, or promoting negative curvature as required to form a fusion stalk; [1,4,9,10] or disrupting the local ordering of the host membrane to facilitate mixing with the viral membrane [1,4,11]. With regard to the latter, prior studies have shown that fusion peptides lower the rupture tension of membranes [12–15]. Molecular simulations have suggested that the fusion peptide of influenza promotes splaying of lipid tails, such that one tail protrudes from the host

* Corresponding author.
E-mail address: mskent@sandia.gov (M.S. Kent).
[1] Current address: Department of Physics, University of Vermont, United States.
[2] JMV and FH contributed equally to this work.
[3] Current address: Department of Chemistry, University of South Florida, United States.
[4] Current address: Bogazici University, Istanbul, Turkey.
[5] Current address: Institute of Zoology, Chinese Academy of Sciences, Beijing, China.

https://doi.org/10.1016/j.bbamem.2018.02.012
Received 3 November 2017; Received in revised form 8 February 2018; Accepted 9 February 2018
Available online 13 February 2018
0005-2736/

membrane, thereby promoting fusion [16,17]. More work is needed to understand fully the detailed mechanisms by which such proteins promote fusion and the roles of their fusion peptides.

In the present work, we studied the fundamental interactions of the soluble portion of the envelope protein of Dengue virus serotype 2 with lipid membranes. Dengue virus (DV) is a flavivirus that is endemic to tropical and subtropical regions of the world [18,19]. The envelope protein (E) is comprised of three domains and is arranged as a head-to-tail dimer in the mature virus, but reorganizes into head-to-head trimers upon exposure to low pH within endosomes [20]. Residues 98-111 comprise the fusion loop (FL) at the tip of the trimer that inserts into the target membrane. While much prior work has focused on the importance of the FL, we show below that positively-charged arginine and lysine residues (R73, K246 and K247) located on the sides of the trimer (within 10 Å from the FL) are also important in the interaction of Dengue E with the target membrane, as suggested recently for the flavivirus St. Louis encephalitis virus [21]. Our simulations indicate that hydrogen bonds formed between these residues and phosphates in the lipid headgroups provide substantially more enthalpic interaction energy than the interaction of the fusion loop with the membrane.

A great deal of evidence indicates that the sequence of the FL of DV is important for fusion, strongly suggesting that the structure, positioning, and specific interactions of the fusion loop within the bilayer are crucial. The amino acid (AA) sequence of the FL is highly conserved among flaviviruses (Fig. S1) [8,14,15,22]. Mutational studies have shown that fusion efficiency is extremely sensitive to various residues in the FL, especially W101, L107, and F108 [7,8,23]. However, the basis for the extreme sensitivity to these aspects is not yet clear. Residues W101, L107, and F108 have been collectively referred to as a hydrophobic anchor [6–8]. But considering membrane binding energies of a large number of peripheral membrane-associated proteins [24] it is surprising that a protein that associates only with the headgroup region of the outer leaflet and inserts only a few hydrophobic residues into the lipid tails will bind irreversibly and remain anchored in the membrane in the presence of large membrane bending stresses that must occur during formation of the fusion stalk. For comparison, a single myristate group (14 carbons) is known to be insufficient to provide stable anchoring to lipid membranes [25–27]. While hydrophobic interactions between the FL and the lipid membrane may contribute to anchoring, the modest interaction energy afforded by three strongly hydrophobic residues (nine in the trimer) and conservation of the structure and sequence of the FL suggests a critical role beyond this.

As is common for enveloped viruses, fusion of flaviviruses has been shown to depend upon the lipid composition of the target membrane. In particular, fusion depends strongly on anionic lipids (AL) and, in the absence of AL, on CHOL [28–31]. Interestingly, the dependence of fusion on CHOL occurs despite lack of a strong association between CHOL and sE [32]. While the viral membrane composition can also impact fusion and will differ for virus produced in different types of cells such as vertebrate and insect cells, we focus here on the composition of the endosomal membrane and its impact on fusion.

In this work, we studied the structure and fundamental interactions of Dengue sE inserted into membranes of 70:30 1-palmitoyl-2-oleoyl-*sn*-glycero-3-phosphocholine (POPC): 1-palmitoyl-2-oleoyl-*sn*-glycero-3-phospho-rac-glycerol (POPG), 49:21:30 POPC:POPG:CHOL, and 49:21:30 POPC:1-palmitoyl-2-oleoyl-*sn*-glycero-3-phosphoethanolamine (POPE):CHOL by neutron reflectivity (NR). We also studied 70:30 POPC:POPG, 1:1 POPC:POPE, and 1:1:1 POPC:POPE:CHOL by molecular dynamics (MD) simulations. This work was motivated by the desire to understand, for flaviviruses, the fundamental bases for i) the critical role of the fusion loop, as indicated by a high degree of conservation; ii) the critical role of AL to fusion, as reported recently; [33] and iii) cholesterol-enhanced binding of sE [30,32], lipid mixing [29,30,33], and fusion [28] (in absence of AL) despite the lack of a strong specific interaction of CHOL with sE [32].

The combined NR and simulation results resolve the depth of insertion, the orientation of sE with respect to the membrane normal, and the fundamental interactions that occur between sE and the lipids. The results show that positively-charged lysines K246 and K247 and arginine R73 in the vicinity of the FL contribute significantly to the interaction. In particular, K246 and K247 each form multiple hydrogen bonds with phosphates of lipid headgroups that cause the trimer to tilt upon insertion. These hydrogen bonds are promoted by both AL and CHOL, but the effect is much stronger for AL. The results suggest that these hydrogen bonds play an important role in membrane anchoring, along with the FL.

2. Materials and methods

2.1. Materials

POPC, POPG sodium salt, POPE, and CHOL were purchased from Avanti Polar Lipids. The HC18 (*Z*-20-(*Z*-octadec-9-enyloxy)-3,6,9,12,15,18,22-heptaoxatetra-cont-31-ene-1-thiol) tethering compound was synthesized at NIST as previously reported [34].

2.2. Expression and purification of DV2 sE

The DV2 construct (strain NGC) used in this work consists of prM and E ectodomain residues 1-395 with single or double strep tag, and has been described in detail elsewhere [35]. This construct was expressed in S2 cells as follows. S2 cells were grown in SFX-Insect medium (Thermo Hyclone). Initially, we used alternative serum-free media (Insectagro-DS2, Life Technologies) but obtained mediocre growth rates relative to other media and poor protein yield. Shaking cultures in 2 L baffled flasks containing 600 mL of medium were inoculated at 3–6 $\times 10^6$ cells per mL and copper sulfate was added at a final concentration of 1 mM on culture day 0. On days 7–9, culture supernatant was harvested by centrifugation at 13,000 $\times g$, 15 min, 4 °C. For each batch, a total of 8 L of clarified and 0.2 μm-filtered supernatant was then concentrated to 1 L using Vivaflow 200 concentrators (Sartorius, 10,000 Da cutoff). Egg white avidin (Life Technologies) was then added to the supernatant at a final concentration of 15 μg/mL to bind free biotin that would interfere with purification, and the pH was slowly adjusted to 8.0 using 0.5 M NaOH with rapid stirring (M = mol/L). During our efforts, we determined that buffer exchange was unnecessary for binding to streptactin and generally caused formation of a crystalline precipitate that clogged the affinity columns. Supernatant was then passed over two 1 mL streptactin columns (Qiagen) in series at a flow rate of 1 mL/min. Columns were washed with 40 mL PBS pH 8 then eluted using 5 mM desthiobiotin (Sigma) in wash buffer. Buffer exchange (1:100–1:500) and concentration were done using centrifugal ultrafiltration and TAN buffer (20 mM triethanolamine, pH 8.0, 130 mM NaCl). Purified protein in TAN buffer was quantified by UV spectrophotometer (NanoDrop2000) using a calculated molecular weight of 46,906 Da and molar absorption coefficient ε of 59,190. Aliquots were stored at −80 °C.

2.3. Preparation of tethered lipid bilayer membranes

Adsorption of sE to tethered bilayer lipid membranes (tBLMs) was studied by NR. tBLMs were prepared on HC18-self-assembled monolayer (SAM)-coated 3′ diameter Silicon wafers (El-Cat Inc., Ridgefield Park, NJ, USA) assembled in a NCNR reflectometry flow cell [36] as previously described [34]. The tBLMs were completed by liposome fusion. Liposomes of the desired composition were prepared as follows. The lipid mixture in either chloroform (49:21:30 POPC:POPE:CHOL) or 90:10 chloroform:methanol (70:30 POPC:POPG, 49:21:30 POPC:-POPG:CHOL) was dried in a clean glass vial using a steady stream of nitrogen gas and then further dried for a minimum of 4 h under vacuum to remove excess solvent. The lipid mixture was then rehydrated for 10 min in a high salt TAN buffer (20 mM triethanolamine, 500 mM

NaCl, pH 8.0) and vortexed for 1 min. Two cycles of hydration and vortex agitation were performed to release all lipids from the vial wall. The liposomes thus formed (2.5 mg/mL) were injected into the measurement cell containing a gold-coated wafer with tethering HC18-SAM, incubated for a minimum of 1 h, and then exchanged with a low salt TAN buffer (20 mM triethanolamine, 50 mM NaCl, pH 8.0).

2.4. Preparation of lipid monolayers at the air-water interface

Adsorption of sE to Langmuir monolayers of either 100% DPPG or a 70:30 mol% mixture of DPPC and DPPG was studied by NR and X-ray reflectivity (XR). The lipids were spread from a mixture of chloroform and methanol on the surface of 20 mM MES buffered H_2O subphase (pH 5.5, 130 mM NaCl) held within a Teflon trough (70 mm × 70 mm × 2 mm). After allowing the chloroform and methanol to evaporate, the surface layer was compressed to the target pressure by a movable barrier. Sufficient lipid was deposited such that after reaching the target pressure the barrier remained outside of the footprint of the X-ray or neutron beam. After collecting XR or NR data for the lipid monolayer alone, sE was then injected into the subphase underneath the lipid monolayer. For the case of a 70:30 mol% mixture of DPPC and DPPG, a stable surface layer of sE bound to the lipid monolayer could not be attained, despite exploring various combinations of surface pressure and sE concentration. However, a stable surface layer of membrane-bound sE resulted for the case of 100% DPPG at a surface pressure 30 mN/m. In that case sE was injected at a concentration of 1.2 μM. After waiting several hours for adsorption to be completed, X-ray reflectivity scans were collected. The trough was maintained at 20 ± 2 °C.

2.5. Background on neutron and X-ray reflectivity

NR and XR are analogous to the more familiar small angle scattering (SAS) methods used to study the structure of proteins and protein complexes in solution [37]. However, in contrast to SAS, NR and XR can be used to study membrane-bound proteins [38]. NR and XR involve measuring the ratio of reflected intensity to incident intensity as a function of momentum transfer $q_z = 4\pi\sin\theta/\lambda$, where θ is the angle of incidence and λ is the wavelength. The form of this curve is determined by the profile of the in-plane averaged neutron or X-ray scattering length per volume, or scattering length density (SLD), normal to the surface [39]. The neutron or x-ray SLD is directly related to the atomic composition and the density of the reflecting body. (Since X-ray SLD is proportional to the electron density, the latter is typically reported rather than the SLD). Therefore, for a protein bound to a planar lipid membrane, NR and XR determines the distribution of amino acid residues normal to the membrane (averaged in-plane) with resolution comparable to that of the corresponding SAS methods (typically 10–20 Å). While the amino acid distribution within a protein is determined to only low resolution, the vertical position of a protein relative to the membrane is determined to a much higher precision [40]. Manipulating the contrast between components within a structure is integral to neutron scattering methods. For organic materials this is readily accomplished using the very different neutron SLD of hydrogen and deuterium.

While some information can be obtained from reflectivity data by inspection, such as determining thicknesses from fringe spacings, a fitting procedure is required to obtain the full SLD profile. Fitting reflectivity data involves generating a model SLD profile, calculating reflectivity from the model profile, and then comparing the calculated reflectivity with the data. Parameters of the model profile are then adjusted until good agreement is obtained. The uncertainty in the fitted parameters is determined by a Monte Carlo resampling procedure [41]. For multicomponent interfacial systems such as the tethered lipid bilayers used here, a method has been developed to fit reflectivity data using structural models comprised of volume fraction distributions of the known chemical components, called composition-space refinement [42]. This method constrains the fits to plausible chemical structures and increases the precision with which molecular components can be localized within the interfacial structure. Molecular models for a protein structure, derived from a crystal structure or from molecular theories, can be incorporated into the fitting analysis by dividing the molecular structure into a stack of slabs normal to the surface and calculating the SLD for each slab from the atomic composition and density. The volume fraction, vertical position within the membrane structure, and tilt angle of the protein can then be determined along with the distributions of the lipid components. Reflectivity data for multiple contrast conditions can be fit simultaneously, which greatly improves the ability to resolve the distributions of different components.

2.6. NR measurements

NR measurements of sE adsorption to tLBMs were performed at the NG7 reflectometer at the NIST Center for Neutron Research (NCNR). Reflectivity curves were recorded for momentum transfer values $0 \le q_z \le 0.25$ Å^{-1}. For each measurement, adequate counting statistics were obtained after 5–7 h. The flow cell allows for in situ buffer exchange; therefore, subsequent measurements were performed on the same sample area. The entire flow cell was maintained at room temperature (RT). After in situ completion of the tBLM, NR data were collected with H_2O buffer (20 mM TAN, 130 mM NaCl) and D_2O buffer in the measurement cell. Buffer exchange was accomplished by flushing 10 mL of buffer through the cell (volume ~1.3 mL) using a syringe. The experiments involving Dengue sE were performed using two protocols. In the first, a 2 mL solution of 1 μM sE in buffer at pH 5.5 was injected into the measurement cell using a syringe and allowed to incubate several hours during which short NR scans were collected to monitor the level of adsorption. This was repeated three times with increased adsorption occurring in each case. Following the fourth injection of 1 μM sE, final scans were collected. This protocol was used with the PC:PG membrane. In the second protocol, following collection of NR data for the tBLM in H_2O and D_2O buffer, a 2 mL solution of a higher concentration of sE (3.4 μM for PC:PG:CHOL and 8 μM for PC:PE:CHOL) in pH 5.5 buffer was injected into the measurement cell using a syringe. For each of these cases, 5% PEG 400 was included to inhibit aggregation of protein and non-specific adsorption of protein to the membrane. Short NR scans were collected until adsorption was completed. The cell was then exchanged with D_2O buffer, and a full scan was collected. Then the cell was exchanged with H_2O buffer and a full NR scan was collected.

The 1D-structural profile along the lipid bilayer normal used to fit NR scans consisted of a stratified slab model for the solid substrate [43], a continuous distribution model for the tBLM [42], and a monotonic Hermite spline for the model-free envelope of the protein [38]. Individual slabs were implemented for the bulk silicon, the silicon oxide, the chromium, and the gold layer. Fit parameters are thickness and neutron scattering length density for each layer, except for the bulk silicon. One global roughness fit parameter applies to all substrate interfaces. Individual sub-molecular groups implemented in the continuous distribution model are: β-mercaptoethanol (βME), tether polyethylene glycol (PEG) chains, tether glycerol groups, substrate-proximal and substrate-distal PC and PE headgroups, substrate-proximal and substrate-distal methylene and methyl chains of lipid and tether molecules that average the volume and scattering properties of all lipids including CHOL. Fit parameters are the bilayer hydrocarbon thickness for each bilayer leaflet, bilayer surface coverage, tether surface density, tether thickness, and βME surface density. A Hermite spline that describes the volume occupancy profile of the protein is defined by control points, which are on average 15 Å apart. The spatial extension of the protein along the bilayer normal determines the number of control points, and is determined iteratively during model

optimization. Fit parameters for each control point are the volume occupancy of the envelope and the deviation from a position defined by equidistant control points throughout the spline. Over the extension of the spline, a constant neutron SLD is applied, which is a function of the bulk solvent SLD taking into account proton exchange of the protein with the bulk solvent. Since reflectivity measures the profile normal to the interface (averaged in-plane), the volume distributions of the various components at each depth through the interface are expressed as cross-sectional areas. The maximum value of the cross-sectional area equals the global area per molecule of that component.

To determine the orientation of the protein at the lipid bilayer, we performed additional fits using rigid structural models for the protein [44]. The structure 1OK8.pdb was used along with a modified structure in which the monomers are splayed to an angle of roughly 52°, as suggested by Klein et al. in the absence of a zipped-up stem region [45]. We refer to the latter structure as "open form." An animation showing the two structures is provided in the Supporting information (Fig. S2). Both structures were aligned with their largest principal axis along the bilayer normal, and with the membrane-binding interface toward the bilayer. The resulting structures define the respective (0°, 0°) orientation. For modeling the NR data, two continuous fit parameters, equivalent to the two Euler angles (β, γ), describe the final orientation of the protein at the interface. Every orientation (β, γ) can be obtained by extrinsic rotations of the protein around the axes of the bilayer coordinate system. First, the protein is rotated by γ about the membrane normal, or the *z*-axis. Second, the protein is rotated by β about the *x*-axis, which is in plane with the membrane. The third Euler angle would correspond to a third extrinsic rotation around the *z*-axis, but NR is invariant to this orientation. The fit allows for orientations within $0° \leq \beta \leq 90°$ and $0° \leq \gamma < 360°$. Data modeling and optimization of model parameters were performed using the ga_refl and Refl1D software packages developed at the NCNR [36]. Optimization of model parameters was achieved by using a differential evolution Markov chain. All reflectivity curves of one data set were fit simultaneously to the same model, sharing fit parameters, for example, for the solid substrate. A Monte Carlo simulation or analysis of the Monte Carlo Markov chain was used to determine the fit parameter confidence limits, avoiding over-parameterization.

NR measurements of sE adsorption to Langmuir monolayers were performed at the NG7 reflectometer at the NIST Center for Neutron Research (NCNR). Reflectivity curves were recorded for momentum transfer values $0 \leq q_z \leq 0.25\,\text{Å}^{-1}$.

2.7. XR measurements

XR measurement of sE bound to a Langmuir monolayer of 100% DPPG was performed using an X-ray reflectometer (Bruker, D8 Advance) employing Cu K_α radiation at NCNR/NIST (Gaithersburg, MD). The copper source was operated at 40 kV and 40 mA, and the wavelength was 0.154 nm. The beam width was 10 mm and the beam height was 0.1 mm.

For the case of a monolayer of 100% DPPG, the XR data were analyzed using the Ga_refl program based on the optical matrix method. Analyses were performed with free form models involving a small number of slabs. The free form models consisted of one layer each for the lipid tails and the lipid headgroups, and one layer for the protein. This was sufficient to achieve a good fit to the data. Since no insertion occurred upon sE binding, as indicated by little or no movement of the barrier, the thickness and SLD of the lipid tail layer after adsorption of sE were constrained to the same values as determined for the data taken prior to adsorption. Lack of change in thickness of the lipid layers is demonstrated by absence of a shift in the fringes. In the Ga_refl program the roughness parameter is the full width at half maximum (FWHM = 2.35 σ, where σ is the standard deviation) of a Gaussian distribution and was constrained in the fitting to be less than the smallest thickness of the two adjacent layers.

2.8. MD simulations

The DV soluble E trimer was simulated based on coordinates from the crystal structure (PDBID: 1OK8 [6], residues 1-144 and 159-394). A truncated model of the sE trimer (residues 59-124 and 229-255) was used to study interactions of the tip and fusion loop of the protein with lipid membranes. The truncated sE model is less than half the length of the full sE trimer and significantly lowers the computational simulation costs. The truncation point was chosen to keep three disulfide bonds (C60-C121, C92-C116, and C74-C105) that help maintain the structure of the reduced model. The full-length and truncated sE trimers were each simulated in solution (including 130 mM NaCl) for 150 ns to compare the structural validity of the truncated model. Protonation states for amino acids in both sE models were chosen based on the results from PROPKA [46] analysis of the crystal structure at pH 5.5.

The truncated sE trimer was simulated with three lipid bilayer systems with varying ratios of POPC, POPE, POPG and CHOL. The PC:PG bilayer was composed of 358 PC and 154 PG lipids (70:30 PC:PG). The PC:PE:CHOL bilayer was composed of 216 PC, 216 PE and 216 CHOL lipids (1:1:1 PC:PE:CHOL). The PC:PE bilayer was composed of 256 PC and 256 PE lipids (1:1 PC:PE). Each bilayer was constructed by random lateral (in the membrane plane) distribution of lipid components in each leaflet, followed by water solvation (including ions) and equilibrated for 400 ns. Two truncated sE trimers were placed on one side of each lipid membrane, with the fusion loop residues of the protein tip within contact distance of the lipid headgroups. The principal axis of each truncated sE trimer was intially oriented along the membrane normal so that the protein was "upright" and perpendicular to the membrane plane. The two proteins were laterally positioned so that the distance between closest atoms was > 1.7 nm. The thickness of the water layer was adjusted in each case to ensure that the upright truncated sE trimer was ~2.0 nm from the other side of the lipid bilayer across the periodic boundary. Ion concentrations were adjusted for each system to have a 130 mM NaCl concentration. All membrane-protein systems were simulated for 600–700 ns, as needed for equilibration.

For the PC:PG and PC:PE:CHOL membranes, an additional "fixed-tilt" simulation was run in which the truncated trimers were contrained to a perpendicular orientation with respect to the membrane (*xy* plane). This condition was achieved by applying a harmonic restraint (force constant of $1000\,\text{kJ} \times \text{mol}^{-1} \times \text{nm}^2$) to the alpha carbons of residues V97, D98, I232 and Q233 of each monomer in the *x* and *y* directions while allowing free motion in *z*.

Protein atoms were modeled with the GROMOS 54A7 forcefield, [47] while the lipid atoms where modeled with the compatible GROMOS 43A1-S3 parameter set of Chiu et al. [48]. Water was modeled with the SPC/E 3-point parameter set [49]. All simulations where conducted with the GROMACS 4.5.7 software package [50]. Pressure was held constant at 1 atm for all systems with a Parrinello-Rahman barostat (isotropically for protein in solution and semi-isotropically for membrane systems). Temperature was held at 298 K with a Nose-Hoover thermostat for all simulations to match the NR experiments except for the fixed-tilt systems. In those systems the temperature was set to 310 K to match physiological conditions. Hydrogen bonds were determined based on a distance criteria of 3.5 Å between the heavy donor and acceptor atoms only, and no angle criteria were included. Lipid splay angle with respect to the membrane normal was calculated by measuring the angle of the vector starting at the center of mass of the phosphorous and *sn*-2 glycerol carbon and ending at the center of mass of the last three carbon atoms of both lipid tails.

3. Results

3.1. NR studies of sE inserted into tethered lipid bilayers

Fig. 1 shows NR data for a 70:30 PC:PG tethered lipid bilayer membrane (tBLM) before and after sE binding. Fig. 1 also shows the

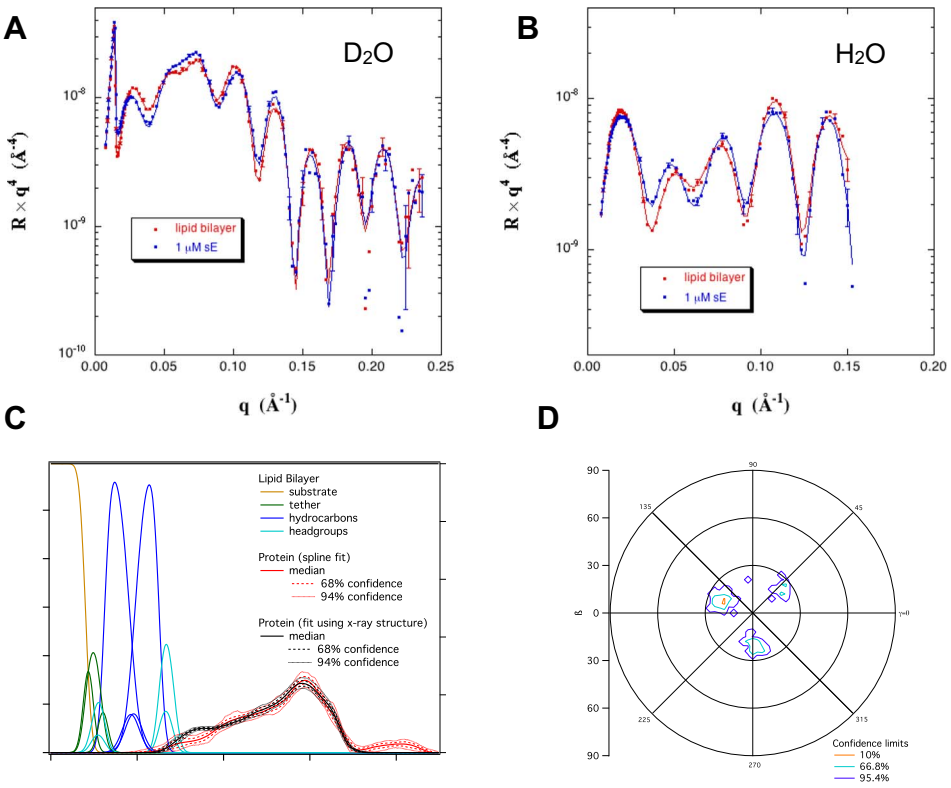

Fig. 1. NR data for E bound to 70:30 PC:PG tethered lipid bilayer in A) D_2O and B) H_2O. Also shown are C) volume occupancy profiles for the different components, and D) angular distributions of sE for the best fits.

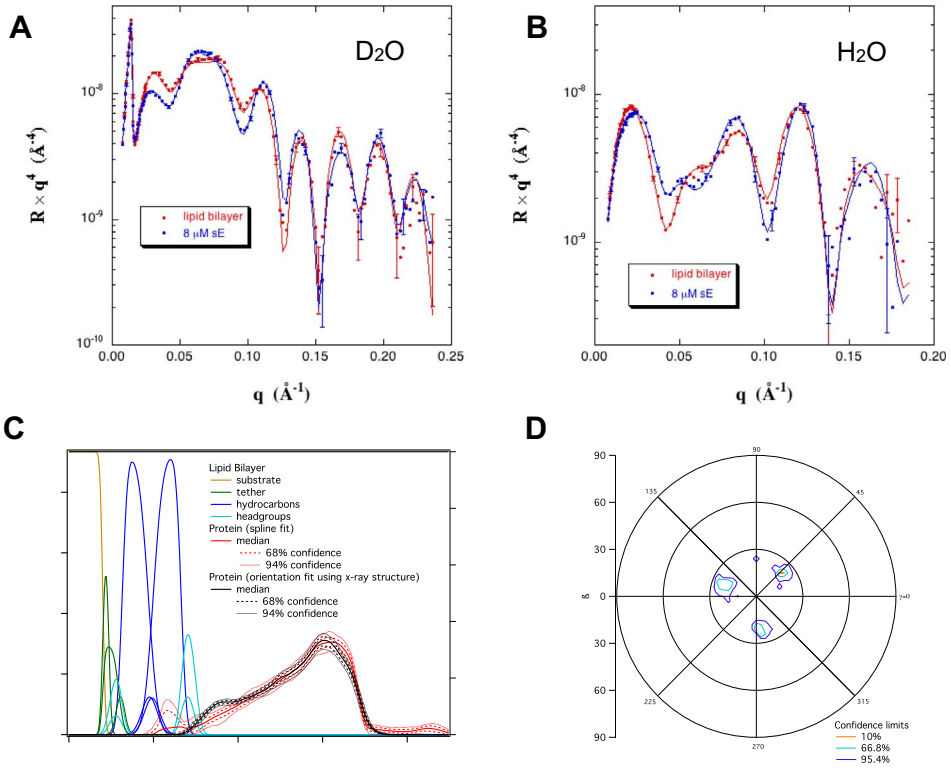

Fig. 2. NR data for E bound to 49:21:30 PC:PE:CHOL tethered lipid bilayer in A) D_2O and B) H_2O. Also shown are C) volume occupancy profiles for the different components, and D) angular distributions of sE for the best fits.

Table 1
Summary of results from fitting the NR data.
Median fit parameters and 68% confidence limits.

Parameter	Spline fit	Fixed orientation x-ray structure fit with closed-form	Orientation fit with the closed-form x-ray structure	Orientation fit with the open-form x-ray structure
70:30 PC:PG				
Bilayer roughness, σ/Å	2.4 ± 0.3	2.9 ± 0.3	2.7 ± 0.3	2.7 ± 0.2
Area per lipid with protein at the interface/Å^2	62.4 ± 1.6	67.1 ± 1.4	63.3 ± 1.9	63.0 ± 1.3
Penetration into lipid bilayer	n/a	16.5 ± 0.6	11.0 ± 1.9	16.6 ± 3.2
Amount of surface-associated protein/ (Å^3/Å^2)	13.5 ± 0.7	11.6 ± 0.4	14.1 ± 0.6	13.6 ± 1.1
χ^2	1.15	1.20	1.12	1.22
49:21:30 PC:PE:CHOL				
Bilayer roughness, σ/Å	3.0 ± 0.3	2.7 ± 0.2	2.5 ± 0.2	2.6 ± 0.2
Area per lipid with protein at the interface/Å^2	55.7 ± 1.5	48.8 ± 0.8	46.9 ± 1.0	48.2 ± 0.8
Penetration into lipid bilayer	n/a	14.3 ± 0.5	8.9 ± 1.4	15.4 ± 2.2
Amount of surface-associated protein/ (Å^3/Å^2)	20.7 ± 1.2	19.0 ± 0.6	17.4 ± 0.9	19.4 ± 0.8
χ^2	1.18	1.27	1.06	1.37
49:21:30 PC:PG:CHOL				
Bilayer roughness, σ/Å	2.5 ± 0.3	2.7 ± 0.2	2.3 ± 0.2	2.4 ± 0.2
Area per lipid with protein at the interface/Å^2	58.3 ± 1.5	52.2 ± 1.2	49.0 ± 1.0	51.7 ± 1.1
Penetration into lipid bilayer	n/a	17.4 ± 0.5	9.6 ± 1.5	21.8 ± 1.6
Amount of surface-associated protein/ (Å^3/Å^2)	26.4 ± 0.9	23.3 ± 0.6	23.5 ± 0.7	24.8 ± 0.6
χ^2	1.07	1.74	1.27	1.26

best-fit model in terms of the volume occupancy profiles of the various components and the angular distribution of sE, where the closed form crystal structure of the sE trimer was used in the fits. Corresponding data for sE inserted into a 49:21:30 PC:PE:CHOL tBLM are shown in Fig. 2. Data for a 49:21:30 PC:PG:CHOL tBLM are provided in Fig. S3. Best fits were independently determined using a free-form Hermite spline that makes no assumptions about the shape of the volume occupancy profile, and also using the X-ray crystal structures of the sE trimer within a rigid body modeling approach. Two crystal structures for the sE trimer have been published, which we refer to as the closed and open forms [6,45]. Both forms were used in the fitting. The fitting results are summarized in Table 1. A complete listing of fit parameters is given in the Supporting information (Table S1).

sE trimer structures were used in the fitting because prior work has shown that sE forms trimers upon insertion into lipid membranes and that nearly all of the inserted protein is in the trimer form [51]. The measurements were performed after incubation at pH 5.5 for > 2 h. This is more than enough time for trimerization of membrane-bound sE [31,32] and for the final form with domain III folded back against domain II to be reached [28,33].

For 70:30 PC:PG and 49:21:30 PC:PE:CHOL, better fits (as measured by the χ^2 values) resulted from using the closed form structure, whereas comparable quality fits were obtained for the open and closed trimer structures in the case of 49:21:30 PC:PG:CHOL. The fitting results show that the final state of the inserted protein is similar for the three membrane compositions. E inserts such that the FL at the tip of the protein coincides with the interface between the lipid headgroups and the hydrophobic tails. The depth of insertion of sE for the different membranes is the same within the uncertainty. For each membrane composition, the fit improves substantially when the orientation of the protein with respect to the membrane normal is allowed to vary (see χ^2 values in Table S1). The tip-inserted protein is tilted with respect to the membrane to a similar degree (up to 30°) for the three membrane compositions. The roughness values of the membrane after sE insertion, which account for fluctuations normal to the membrane, are also the same for the different membranes within the uncertainty. The values indicate little increase in membrane fluctuations or roughness upon binding of sE.

3.2. NR and XR studies of sE adsorption to lipid monolayers at the air-water interface

Adsorption of sE to Langmuir monolayers of either 100% DPPG or a 70:30 mol% mixture of DPPC and DPPG was also examined by NR and XR. For the case of a 70:30 mol% mixture of DPPC and DPPG, a stable surface layer of sE bound to the lipid monolayer could not be attained, despite exploring various combinations of surface pressure and sE concentration. Rather, under conditions for which insertion of sE occurred as detected by backward movement of the barrier, insertion continued until the barrier reached the back of the trough. Analysis of the NR or XR data indicated that sE had inserted fully into the lipid layer and was exposed to the air interface, rather than extending from the lipid layer into the subphase as observed with lipid bilayers in Figs. 1 and 2. Since the presence of the air interface clearly affected the adsorption and insertion process, we concluded that Langmuir monolayers are not an adequate mimic of the outer leaflet of a lipid bilayer with respect to studying the membrane-inserted structure of sE. However, for the case of 100% DPPG, a stable surface layer of adsorbed sE was obtained. In that case, virtually no movement of the barrier resulted, indicating little or no insertion of sE. XR data collected for this case are shown in Fig. 3 along with the fitting results. The electron density profile is qualitatively different from the profiles of sE inserted into bilayers shown in Figs. 1 and 2. The results could be fit using a single layer for the protein below the lipid headgroups (i.e., in the water layer) with an average thickness of 38 Å followed by a diffuse tail extending into the subphase. This structural data, combined with the absence of insertion (lack of increase in area), indicates that sE adsorbed side-on to the lipid headgroups. While a composition of 100% DPPG is not representative of the outer leaflet of a biological lipid bilayer, we include this data here because it demonstrates that sufficiently strong electrostatic interactions with the membrane will cause sE to adsorb in a side-on orientation. This observation will contribute to the discussion below.

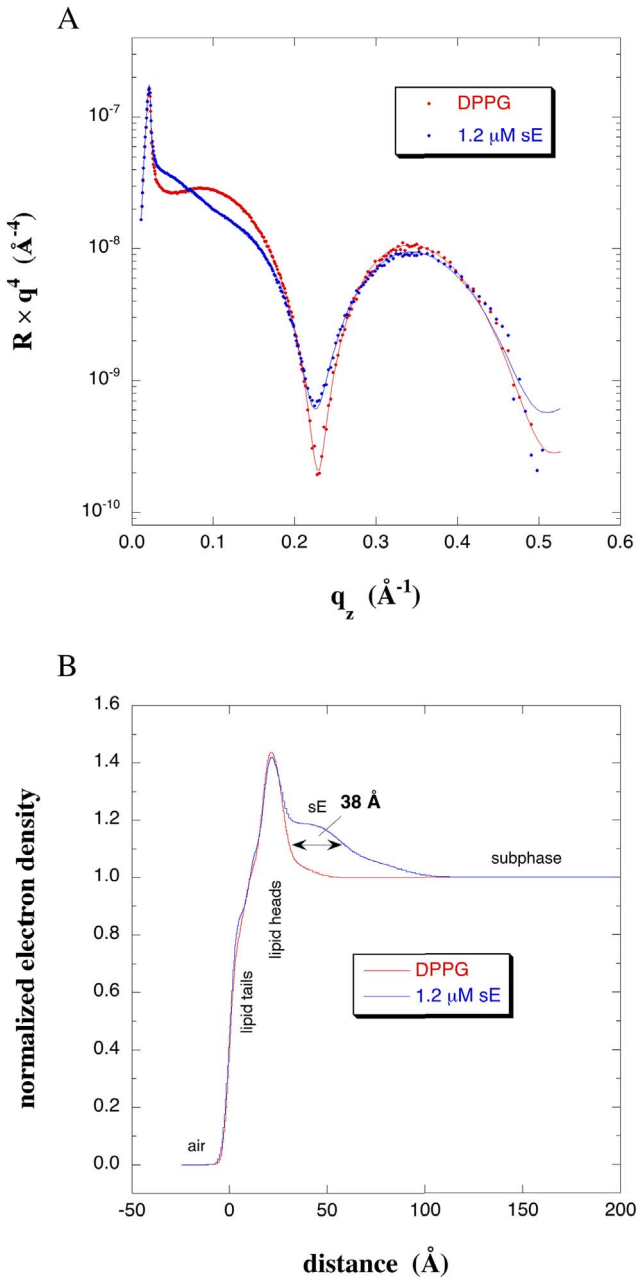

Fig. 3. A) X-ray reflectivity data and B) fitted electron density profiles for sE binding to a monolayer of 100% DPPG in a Langmuir trough. The profile is entirely different from that in Figs. 1-2, and shows that in the unrealistic case of a membrane of 100% AL the electrostatic interactions with positively-charged residues exposed on the surface of sE are sufficiently strong to cause the protein to adsorb in a side-on orientation.

3.3. Simulations of sE trimer with lipid membranes

We characterized the molecular level interactions between Dengue sE trimer and lipid membranes with atomistic MD simulations. The large size of the trimeric protein (> 1000 AAs with a length > 100 Å, see Fig. 4A) would require excessive computational resources at the atomic level of description. Therefore, we developed a truncated sE trimer model (residues 59-124 and 229-255) based on the crystal structure of the closed form (see Fig. 4B and Methods for details). The truncated portion used in the simulations contained the FL and all residues within 45 Å of the FL. To validate this model, a 150 ns simulation was run for the truncated structure in solution (no lipid membrane) with pH 5.5 amino acid protonation states. The truncated trimer (TT) in solution is highly stable, and maintains a similar structure compared to the full sE trimer (Fig. 4). While the TT is slightly more compact near the truncation regions, the structure of each individual monomer (Fig. 4C) as well as the FL region for the TT remain close to the crystal structure, as shown in the root-mean-squared deviation plots (Fig. 4D).

Two distinct TT structures, each taken from the solution-equilibrated simulations, were brought into contact with pre-equilibrated lipid membranes (512-648 lipids, see Methods) of three different compositions (1:1 PC:PE, 1:1:1 PC:PE:CHOL, and 70:30 PC:PG). Each TT was placed in a vertical orientation (long axis perpendicular to the membrane plane and FL in contact with lipid headgroups, Fig. 5) and simulated for 600–700 ns. During each simulation, the TTs in most cases adopted a tilted orientation with respect to the membrane. Time-dependent changes in the tilt angle, hydrogen bonds, and depth of insertion are shown in Fig. 5 for the two trimers at each of the three membrane compositions. The depth of insertion is defined as the distance from the center of mass of residue W101 with respect to the center of mass of the phosphate groups of neighboring lipids (those in contact with the protein). The magnitude of the tilt is comparable for PC:PE:CHOL and PC:PG, but considerably weaker for PC:PE. Tilt angle is strongly correlated with the number of hydrogen bonds that each TT establishes with the neighboring lipids. For each membrane composition, the largest number of hydrogen bonds occurs with the phosphate oxygens of the lipid headgroups (Fig. 6). The PG glycerol moiety, and to a lesser extent the PE NH_3, also provide a significant contribution to the overall protein-lipid hydrogen bonding (Fig. 6). As the tilt angle (θ) of the TTs increases beyond 20–30°, the Lys and Arg residues at the periphery of the protein (especially K246, K247, and R73 near the FL) establish a significant number of hydrogen bonds (~25% of all hydrogen bonds, Fig. 7). Most of the lysines that contact the lipid headgroups form 2-3 hydrogen bonds with the phosphate oxygens, as depicted in Fig. 7E. Interestingly, K110 in the fusion loop only rarely forms hydrogen bonds with the lipids due to the fact that it is buried at the interface of the three monomers and forms hydrogen bonds with nearby protein residues instead.

While there is a preference for TT to hydrogen bond PG and PE lipids over PC (Fig. S3), the ratios of protein-lipid contacts (Fig. S3) do not show any clear pattern of clustering or lipid segregation around the proteins. The TTs have few interactions with cholesterol molecules due to the fact that cholesterol is located in the lipid tail region and does not extend into the lipid headgroups (Figs. S4 and S5). However, the highly conserved (Fig.S1) W101 is located in the fusion loop (Fig. 5, schematic, bottom left panel) and penetrates significantly more deeply into the PC:PE:CH membrane compared to the other compositions (Fig. 5, bottom panels). This deeper insertion is facilitated by rare contacts with cholesterol molecules (Fig. S5). Increased tilt and hydrogen bonding in the PC:PG and PC:PE:CHOL membranes may also contribute to the deeper insertion of W101 compared to PC:PE (Fig. 5, bottom panels).

Since the protein-membrane interactions induce tilting of bound trimers, we wondered if the membrane would bend around a TT that is not free to tilt. To answer this question, we simulated the trimers with PC:PG and PC:PE:CHOL membranes while fixing the orientation (see Section 2.8 for details) of each TT to remain perpendicular to the membrane plane (tilt angle < 10°, Fig. 8). The polar interactions and hydrogen bonding for the PC:PG fixed-orientation simulation result in a large deformation of the membrane as the lipids wrap around the tip of the TT (Fig. 8B). The highest total number of hydrogen bonds (127 ± 7) between the vertically fixed TT and the membrane is the same as for the simulation in which the TT is free to tilt (127 ± 5). The number of hydrogen bonds formed by the positively-charged Lys and Arg residues (K246, K247, R73 and R99, Fig. 8C) is again a significant fraction of the total. R99 forms a similar number of hydrogen bonds as R73, in contrast to the free tilt case. In the case of PC:PE:CHOL, the stiffer membrane does not undergo significant deformation during the simulation time (Fig. 8E), which limits the number of hydrogen bonds (57 ± 6) with the neighboring lipids compared to the free system (118 ± 3). However, K246 and K247 still form some hydrogen bonds

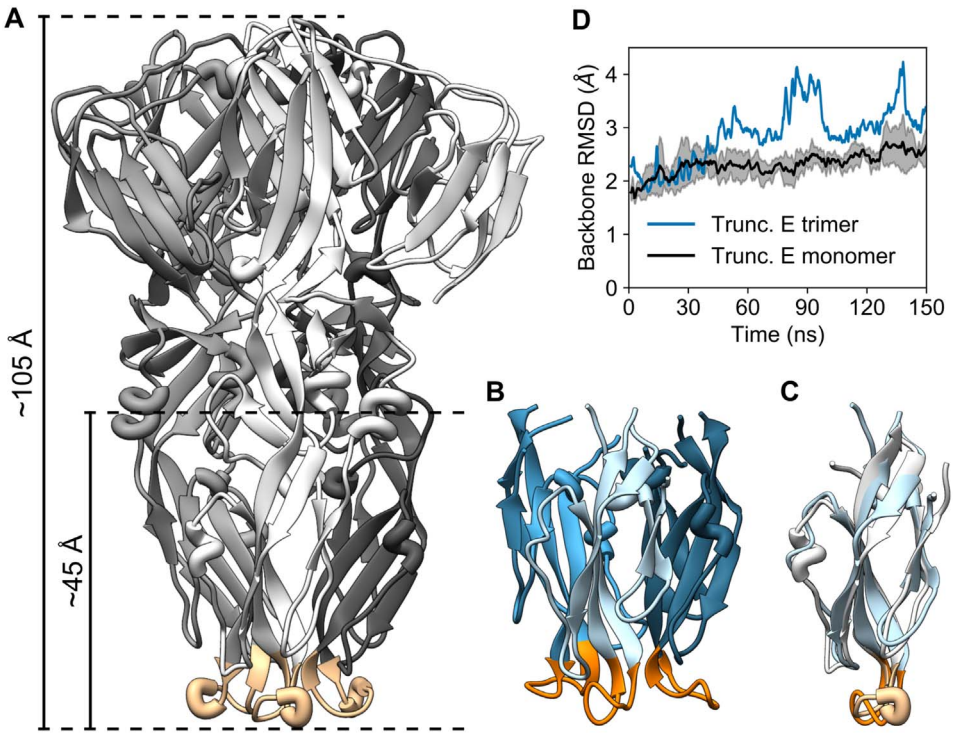

Fig. 4. Truncated E trimer compared to full E trimer in solution. A) Crystal structure of E trimer showing the truncated model (bottom, ~45 Å), including the fusion loop (tan region). B) Truncated trimer structure after 150 ns simulation. C) Best fit of simulated truncated monomer (simulated as trimer) overlaid on crystal structure of complete monomer. D) Root-mean-squared deviation of truncated trimer backbone atoms relative to the crystal structure (for fusion loop region) and average of the three monomers (all residues) compared to the crystal structure.

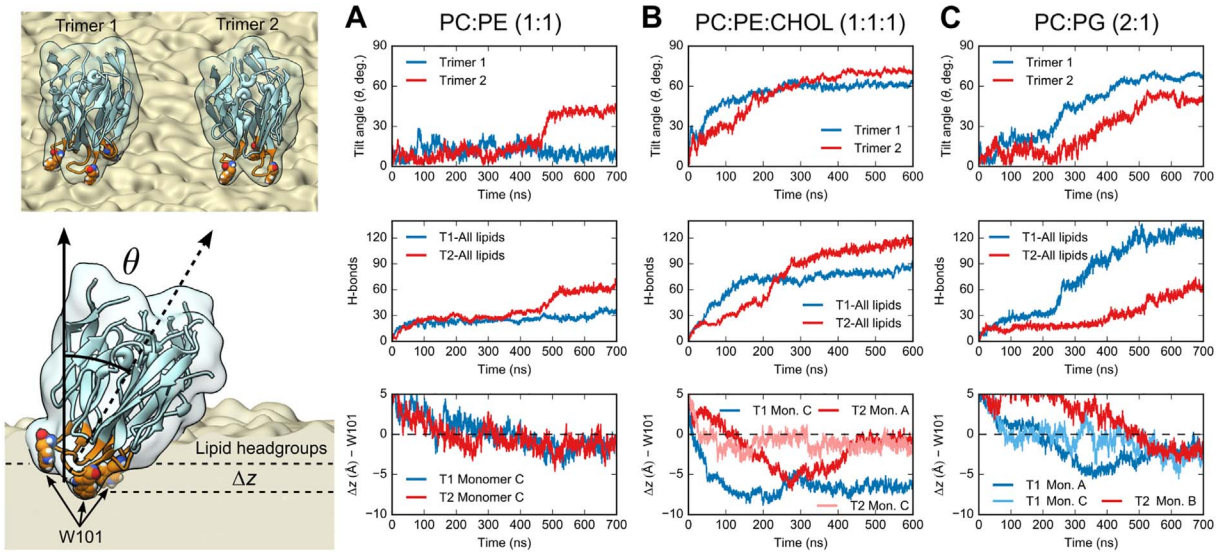

Fig. 5. Tilt angle, number of hydrogen bonds, and W101 depth of insertion (Δz, with respect to surrounding lipid headgroups) of simulated truncated E trimers on (A) PC:PE, (B) PC:PE:CHOL, and (C) PC:PG lipid membranes as a function of time. Truncated E trimers positioned in contact with PC:PE:CHOL and PC:PG lipid bilayers show increased tilt ($\theta \sim 0$ at t = 0) over time. The bottom panels only show data for W101 residues that penetrate below the headgroup region for clarity. Number of hydrogen bonds and depth of insertion are correlated with tilt angle and membrane composition.

with neighboring lipids (Fig. 8F).

To further characterize the protein-membrane interactions, we computed the approximate interaction energies due to van de Waals and short-range Coulomb (up to 1 nm away) forces between each TT and the lipid bilayer, as shown in Table 2. Note that these are not free energies of binding as they do not include entropic terms and have limited statistics, yet they provide a useful qualitative comparison. In the case of the largely tilted TT, the interaction energies are similar for the PC:PG and PC:PE:CHOL cases with the FL-membrane interactions providing ~20% of the total energy. The total interaction energy for the lower tilt TT in PC:PE is significantly smaller (−1042 kcal/mol) compared to the energy of the other membrane compositions (−1693 to −1768 kcal/mol). The contribution from the FL is slightly larger due to a larger number of FL residues in contact with the membrane at the lower tilt. When the protein is fixed in a vertical orientation, the interaction energy for the PC:PG case (−1707 kcal/mol) remains similar to that of the free tilt case, as expected given a similar number of protein-lipid hydrogen bonds. However, for the PC:PE:CHOL system, the protein-membrane interaction energy with the TT fixed in vertical orientation is significantly smaller (−880 kcal/mol) than for the simulation in which the protein is free to tilt. These comparisons indicate that FL-membrane interactions are a minor contribution to the total enthalpic interaction energy when AL or CHOL are present to facilitate hydrogen bonding of K246, K247, R73, and R99 with lipid headgroups. While these enthalpic comparisons do not include the potentially important entropic contribution from solvent reorganization, they

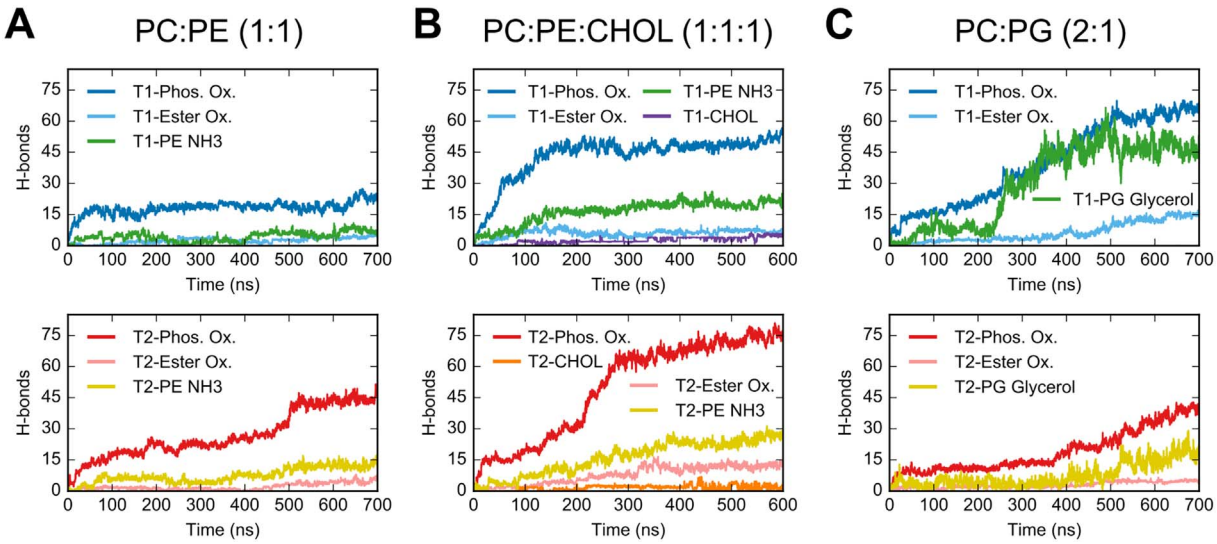

Fig. 6. Number of hydrogen bonds between the truncated E trimers and the various chemical moieties in the lipid headgroups (phosphate oxygens, ester/glycerol backbone oxygens, ethanolamine NH_3, cholesterol OH, and PG glycerol).

strongly suggest that hydrogen bonding of K246, K247, R73, and R99 with lipid headgroups contributes greatly to the binding energy, along with the FL. The simulations also show that CHOL limits membrane bending, which may slow fusion.

To further examine the importance of K246 and K247 in the membrane interaction, analogous simulations were performed for the TT with mutations K246A and K247A. For a free K246A/K247A TT interacting with a PC:PG (2:1) membrane, the tilt angle as a function of time during the simulation is shown in Fig. 9a, and the total number of hydrogen bonds per TT is 38 ± 4. Both the tilt angle and the number of

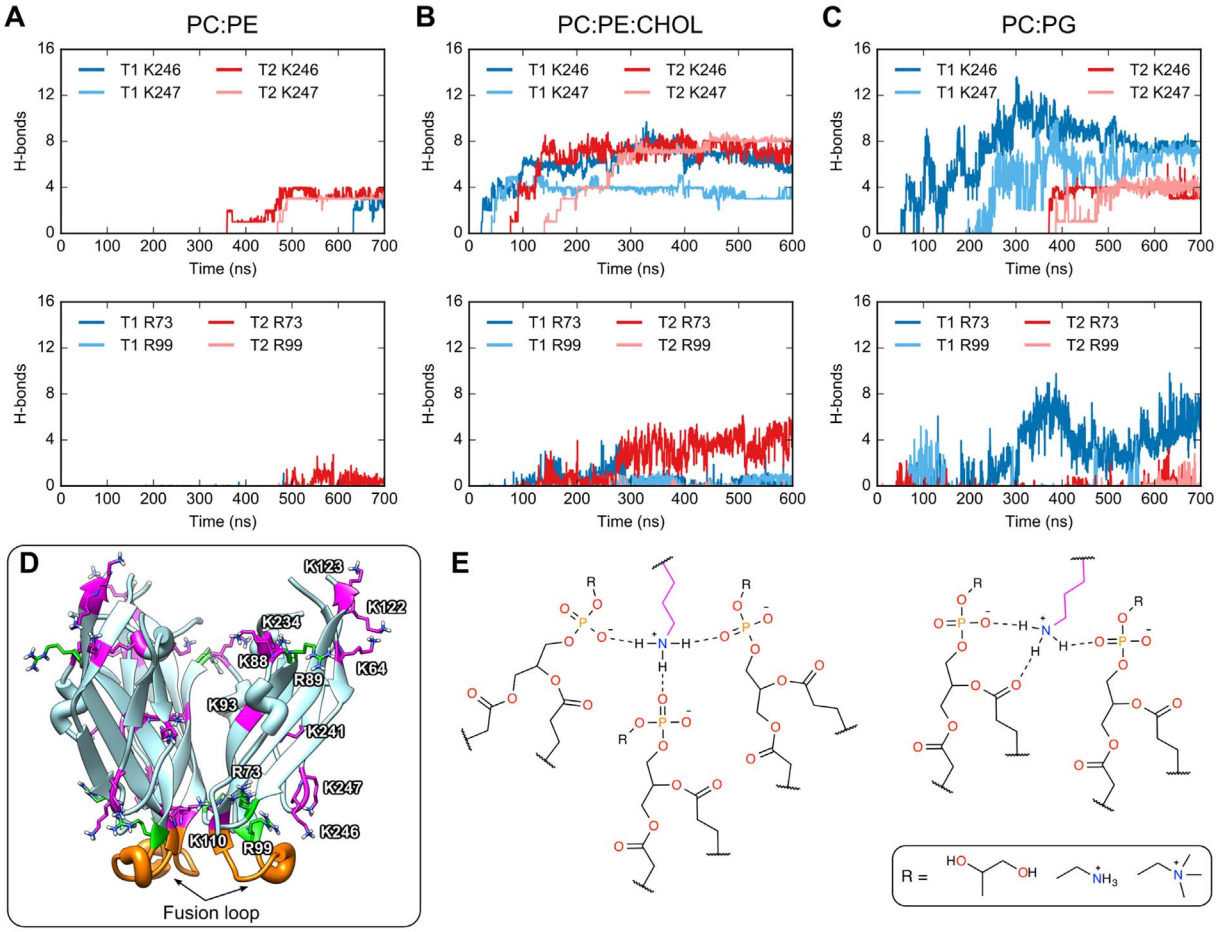

Fig. 7. Characterization of hydrogen bonding between positively-charged residues (K246, K247, R73, R99) near the FL of truncated E trimers and neighboring lipids for the PC:PE (A), PC:PE:CHOL (B), and PC:PG (C) systems. D) Structure of the tip of the TT showing the location of all Lys and Arg residues. E) Common hydrogen-bonding configurations of Lys to the phosphate and ester oxygens in the lipid headgroups.

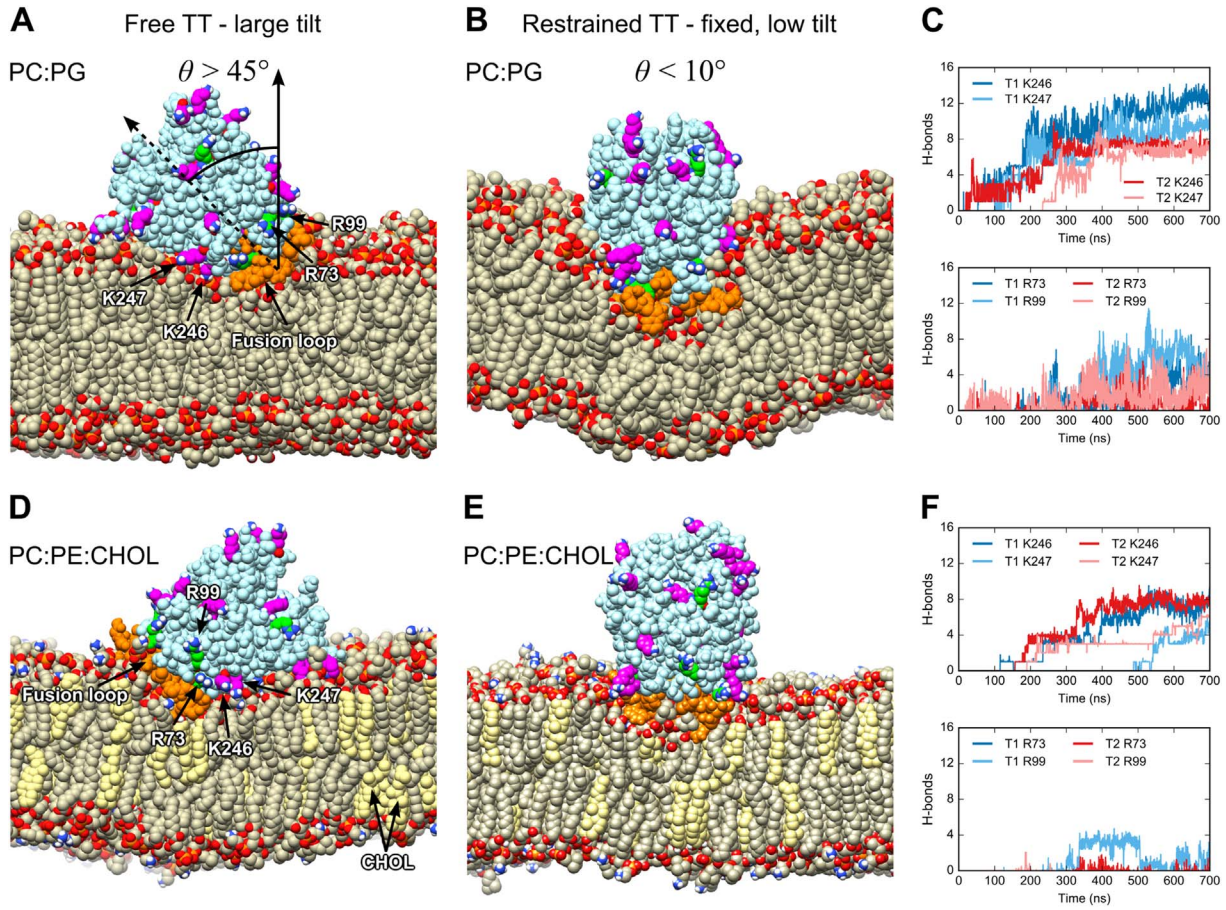

Fig. 8. Simulation cross-section of free (A) and harmonically restrained (B, fixed in vertical orientation, θ < 10°) truncated trimers interacting with PC:PG. C) Hydrogen bonds of positively-charged resides (K246, K247, R73, R99) near the FL and neighboring lipids. Simulation cross-section of free (D) and harmonically restrained (E) truncated trimers interacting with PC:PE:CHOL. F) Hydrogen bonds of positively-charged resides near the FL and neighboring lipids. Lipid carbon atoms are shown in tan color, cholesterol atoms in yellow, protein atoms in cyan except fusion loop (orange), Lys (magenta), and Arg (green) residues. H-bonds between the fixed trimer and neighboring lipids in the PC:PG case result in large deformation of the membrane (B).

Table 2
Approximate protein-membrane interaction energies (kcal/mol)[a].

Membrane comp.	WT sE TT		K246A/K247A TT mutant	
	All AA[b]	FL AA only	All AA[b]	FL AA only
PC:PE	−1042 ± 28	−464 ± 11	–	–
PC:PE:CHOL	−1693 ± 25	−360 ± 12	−414 ± 18	−373 ± 16
PC:PG	−1768 ± 22	−370 ± 11	−608 ± 25	−536 ± 20
PC:PE:CHOL (fixed tilt)	−880 ± 19	−506 ± 15	−681 ± 22	−564 ± 15
PC:PG (fixed tilt)	−1707 ± 27	−626 ± 11	−809 ± 34	−556 ± 17

[a] Includes all van der Waals interactions and any Coulombic interactions up to 1 nm away from protein.
[b] AA stands for amino acids.

hydrogen bonds formed are strongly reduced compared with the results for wild type TT in Fig. 5. Fig. 9B shows the cross section from a simulation at 700 ns in which K246A/K247A TT was fixed in a vertical orientation with respect to the membrane. The membrane does not deform to wrap around the tip of K246A/K247A TT to nearly the extent as for the wild type TT shown in Fig. 8B. The total number of hydrogen bonds between the K246A/K247A TT mutant is 63 ± 6 – roughly half of the number observed for the wild-type case. The lower number of hydrogen bonds results in a substantial reduction in the interaction energies across all systems (Table 2).

The effects of the interactions of the TT and K246A/K247A TT on the splay of the lipid tails that are located near the inserted tip is shown in Fig. 10 for simulations in which the TTs were fixed in a vertical orientation with respect to the membrane. Results are shown for TT interacting with PC:PE:CHOL and PC:PG, and for K246A/K247A TT interacting with PC:PG. The results show that the distortion of the membrane in wrapping around the tip of the trimer for the case of TT interacting with PC:PG corresponds to a significant increase in the splay angle. This suggests that hydrogen bond formation between K246 and K247 and the lipids contributes to destabilization of the membrane.

4. Discussion

NR provides a high-resolution measurement of the depth of insertion of Dengue E trimers into lipid bilayers, and also the first measurement of the orientation distribution of the trimers with respect to the membrane normal. The NR results show that the tip of the protein, which contains the fusion loop, is located at the interface between the headgroups and the hydrophobic tails of the outer leaflet. The depth of insertion is the same for PC:PG:CHOL, PC:PE:CHOL, and PC:PG within experimental uncertainty. Protein adsorption was not detected for PC:PE for the same sE concentration range as used for PC:PE:CHOL, and so NR data were not obtained in that case. The depth of insertion is consistent with the prediction of Modis et al. [6], who argued that W101 and F108 of the fusion loop would penetrate about 6 Å into the hydrocarbon tails and that the depth of insertion into the hydrocarbon tails would be limited by the exposed carbonyls and charged residues on the outside rim of the bowl formed by the fusion loops. A new finding from the present measurements is that E is not oriented normal

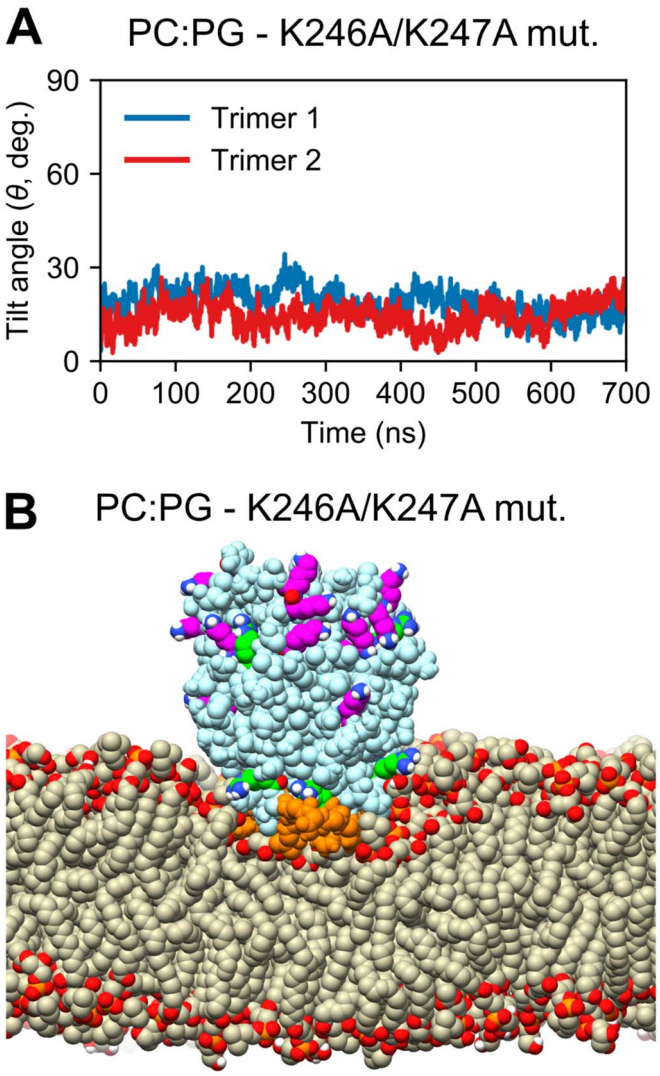

Fig. 9. A) Tilt angle of simulated truncated E trimer K246A/K247A mutant on PC:PG lipid membrane as a function of time. B) Simulation cross-section of truncated E trimer K246A/K247A mutant interacting with PC:PG with fixed protein vertical orientation ($\theta < 10^{\circ}$) with respect to the membrane normal. No significant membrane deformation is observed compared to the wild-type case (Fig. 8B). System was simulated for 700 ns. Color scheme is the same as in Fig. 8.

to the membrane, but rather tilts with respect to the membrane normal (up to 30° under the experimental conditions). The amount of tilt is the same within experimental uncertainty for the three membrane compositions.

The simulations provide atomic resolution as well as insight into the detailed molecular interactions. As expected, hydrophobic interactions of W101 and F108 with the lipid tails promote insertion of the FL into the lipid acyl chain region. Insertion of the tip of sE into the lipid membrane is also promoted by hydrogen bonding of residues with the lipid headgroups. An important new insight from the simulations is the formation of hydrogen bonds between K246, K247, and R73 and the phosphate oxygens in the lipid headgroups. K246, K247, and R73 are located near the tip of the trimer in the vicinity of the FL (Fig. 7D). These interactions induce tilting of the protein with respect to the membrane normal as well as deeper insertion. The simulations show that both CHOL and PG promote protein tilt and hydrogen bond formation. This observation is consistent with the present and previously reported trends in binding affinity and in fusion for flaviviruses. Our experimental results show little binding affinity of sE in the absence of either CHOL or AL, whereas binding affinity increased substantially with 30% CHOL and increased even more strongly with 30% PG. A strong dependence of sE binding affinity on the content of AL has been reported previously [31,33]. Fusion of DV with membranes has also been reported to be strongly promoted by AL [33]. In absence of AL, binding affinity of sE with membranes [30] and lipid mixing and full fusion of flaviviruses [28–30] have been shown to increase with CHOL content. The experimental finding that the binding affinity was much greater for 30% PG than for 30% CHOL in the present study indicates that AL promote binding and fusion more strongly than CHOL on a per mole basis. This is consistent with prior work that showed no dependence of fusion on cholesterol in the presence of AL [32].

While our simulations cannot probe the capture (and binding affinity) of sE trimers to the membrane due to inherent limitations in length and time scales, they indicate that AL and CHOL both promote H-bonding of TT to the membrane to a similar extent. This result, which contrasts with the experimental observation of a stronger increase in binding affinity with AL than with CHOL, may reflect the fact that the simulations began with the TT in contact with the membrane whereas the experimental study includes the full adsorption and insertion processes. Electrostatic interactions involving AL will likely promote absorption of sE to the membrane from solution.

While both PG and CHOL promote the formation of a substantial number of hydrogen bonds between sE and the lipid membranes (up to 128 per trimer), their mechanisms of action differ. PG promotes H-bonding with sE through direct interactions. The glycerol headgroup in PG is a better H-bond donor/acceptor and is less bulky compared to the choline moiety in PC. The net negatively-charged phosphate oxygens of PG also participate in electrostatic interactions with the positively-charged K246, K247, R73, and R99 residues. In the case of CHOL, the effect is indirect. CHOL resides within the lipid tail region, increasing the distance between the lipid headgroups. This is entirely consistent with the well-known condensing effect of CHOL on lipid tails [52]. While the presence of CHOL in the tails causes the lipid tails to extend, decreasing the cross-sectional area occupied by the hydrocarbon chains of each lipid, the average distance between lipid headgroups increases due to the volume occupied by cholesterol. In the MD simulations, the total area divided by the number of phospholipids is ~14% greater for

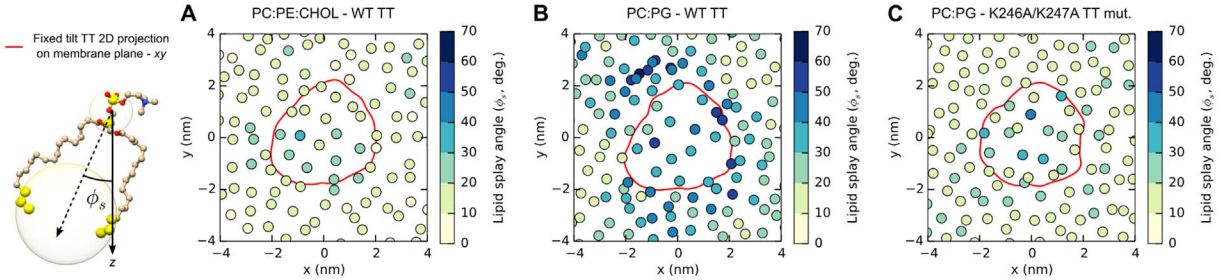

Fig. 10. Splay angle (with respect to the membrane normal, see inset on the left) of lipids for simulations in which the TT was fixed in a vertical orientation for A) wild-type TT interacting with PC:PE:CHOL, B) wild-type TT interacting with PC:PG, and C) K246A/K247A TT mutant interacting with PC:PG. For each lipid the average value over the last 50 ns of the simulation is shown.

the PC:PE:CHOL system (67.9 Å^2) compared to the PC:PE bilayer (58.3 Å^2), whereas the cross-sectional area per lipid for PC:PE:CHOL (45 Å^2) is less than that for PC:PE (58 Å^2) due to the condensing effect of CHOL. This increased area available per phospholipid headgroup provides greater access to the phosphate oxygens of the lipid headgroups for hydrogen bonding. While the large number of interactions promoted by both PG and CHOL facilitate insertion of the FL into the membrane, the simulations show that rare direct contacts between W101 and CHOL also promote partitioning of this residue within the hydrophobic core of the bilayer. Direct contacts are rare because the location of CHOL within the lipid tails provides little access to CHOL's hydroxyl groups. The finding that direct contacts are rare in the simulations is consistent with the previously reported experimental result that CHOL did not associate strongly enough with E to be labeled by photocholesterol or to coextract with CHOL [32].

The fact the CHOL promotes hydrogen bonding though an indirect mechanism explains the previously enigmatic findings that, in absence of AL, CHOL promotes membrane binding [30,32], lipid mixing [29,30,33], and full fusion [28] despite absence of a strong interaction between CHOL and E [32]. An alternative hypothesis was proposed for the indirect role of CHOL in promoting binding of sE to membranes and for a lack of CHOL dependence in fusion of DV to C6/36 mosquito cells [32]. Note that C6/36 mosquito cells contain AL in the outer membrane. Umshankar et al. proposed that CHOL facilitates clustering and trimerization, and thereby stable membrane binding of sE whereas, in absence of CHOL, sE remains monomeric and the binding energy is insufficient for stable membrane binding. They argued that since E is clustered on virus particles, CHOL is not required for trimerization, stable membrane binding, and fusion, consistent with the lack of CHOL dependence for fusion of DV with C6/36 mosquito cells [32]. While this hypothesis is consistent with the data for membrane binding of sE, it is not consistent with the observation that lipid mixing [29,30,33] and full fusion [28] are promoted by CHOL in flaviviruses in absence of AL. We argue here that the lack of CHOL dependence for fusion of DV with C6/36 mosquito cells is due instead to the presence of high concentrations of AL in these membranes. AL promote hydrogen bond formation more strongly than CHOL such that CHOL has little effect on fusion in the presence of AL. Our simulations showed no evidence for clustering of sE in the presence of CHOL, but such an effect might occur on a much longer timescale.

Regarding the relevance of these new findings to fusion, we note first that a region of positively-charged residues containing at least one lysine near the tip of E is common to nearly all flaviviruses, and that R73 and R99 are also highly conserved among flaviviruses, as shown in Fig. 11 [21]. Our simulations show considerably fewer hydrogen bonds formed by R99 in most cases compared to K246, K247 and R73. R99 lies within the FL and may play a role in FL structuring [53], and that may explain the high degree of conservation of that residue. It is not clear at what stage hydrogen bonding interactions form between K246, K247, and R73 and the lipid headgroups, but there is good reason to conclude they will form at the latter stage of fusion, if not earlier. As domain III and the stem segment fold against the body of the trimer, the transmembrane (TM) region of E and target membrane-anchored tip will approach and a dimple will form in the target membrane as illustrated in Fig. 12 [3], creating a shallow angle between the envelope protein and the membrane. We propose that hydrogen bonds form between K246, K247, and R73 and the lipid headgroups at this stage, if not earlier, and provide strong anchoring at the stage of large target membrane bending. However, the interactions may form earlier. If the

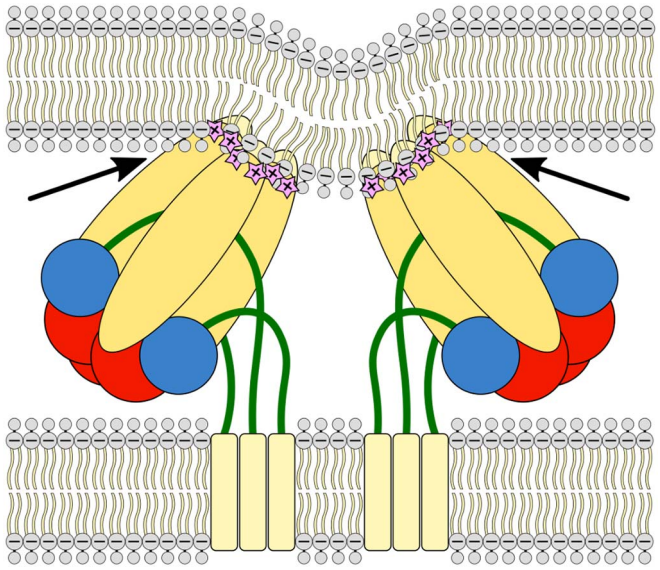

Fig. 12. Illustration showing that a shallow angle (arrows) must form between E trimers and the target membrane as domain III and the stem segment fold against the E trimer. We propose that hydrogen bonds between K246 and K247 and the lipid headgroups form at this stage and strongly anchor the trimer into the membrane to support membrane bending. Tilting of the trimers may also promote membrane destabilization through relocation of the FL or if the target membrane wraps around the tip of the E trimers as in Figs. 8 and 9.
(Adapted from [3]).

	70	80	90	100	240	250
Dengue 1	TDSRCPTQGEATLVEEQDANFVCRRTFVDRG				VTFKTAHAKKQEVVVLGSQ	
Dengue 2	TDSRCPTQGEPSLNEEQDKRFVCKHSMVDRG				VTFKNPHAKKQDVVVLGSQ	
Dengue 3	TDSRCPTQGEAVLPEEQDQNYVCKHTYVDRG				VTFKNAHAKKQEVVVLGSQ	
Dengue 4	TATRCPTQGEPYLKEEQDQQYICRRDVVDRG				VTFKVPHAKRQDVTVLGSQ	
Powassan	VEARCPTTGPATLPEEHQANMVCKRDQSDRG				VEFGPPHAVKMDIFNLGDQ	
Culex	STDVCPGGSQLNMGEINGKERVCSTQPYNRG				VVWGDARANEVLVKNILEP	
Kyasanur	VVARCPAMGPATLPEEHQASTVCRRDQSDRG				VEFGEPHAVKMDIYNLGDQ	
Yellow Fever	INDKCPSTGEAHLVEENEGDNACKRTYSDRG				VEFEPPHAATIRVLALGNQ	
TBE	VAARCPTMGPATLAEEHQSGTVCKRDQSDRG				VEFGAPHAVKMDVYNLGDQ	
SLEV	TVARCPTTGEAHNTKRSDPTFVCKRDVVDRG				VEFEEPHATKQTVVALGSQ	
West Nile 2	TKAACPTMGEAHNEKRADPAFVCKQGVVDRG				MEFEEPHATKQSVVALGSQ	
West Nile 1b	TKAACPTMGEAHNDKRADPSFVCKQGVVDRG				MEFEEPHATKQSVIALGSQ	
Chaoyang	VESGCPGTDEIHNTKAKDTSYMCKVSYPDRG				VEFGVPHATRQSVYSIGDQ	
Usutu	TVSNCPTTGEAHNPKRAEDTYVCKSGVTDRG				LEFEEPHATKQSVVALGSQ	
Donggang	SVNGCPSTTEAHNDKRKDSTYLCERSYPDRG				VEFSTPHATKQSVYTLGDQ	
JEV	TVARCPTTGEAHNEKRADSSYVCKQGFTDRG				MEFEEAHATKQSVVALGSQ	
Zika	SDSRCPTQGEAYLDKQSDTQYVCKRTLVDRG				VEFKDAHAKRQTVVVLGSQ	

Fig. 11. Alignment of flavivirus sequences showing conservation of positively-charged residues R73, R99, K246, K247 shown in this work to form hydrogen bonds with phosphate oxygens of the lipid headgroups.

orientational degrees of freedom of E on the surface of the virus are not constrained, E will tilt upon membrane binding to form these interactions as observed for sE in our experimental and simulation studies. If the orientational degrees of freedom of E are constrained and if the membrane of the host cell is sufficiently flexible, upon membrane binding the target membrane will wrap around the tip of the protein and form these interactions as shown in our simulations (Fig. 8B). Such large local deformation of the membrane could serve to promote fusion of the outer leaflet of the host membrane with the viral membrane (Fig. 10).

An alternative hypothesis for the role of AL was proposed previously by Zaitseva et al., wherein AL promote trimerization of E [33]. They concluded that membrane-associated E forms a “restricted hemifusion” (RH) intermediate [54–56] that does not progress to full fusion until AL are present in late endosomes. In their proposed model, upon acidification in early endosomes, dimers of E dissociate and monomers of E insert into the endosomal membrane. They proposed that membrane-associated E remains monomeric in absence of AL, resulting in a structure that does not support mixing of the outer leaflets, and that AL present in late endosomes facilitate trimer formation and progression to fusion. Since the present simulations were performed with trimers rather than monomers, they provide no evidence for or against the hypothesis that AL promote trimerization of E. However, we suggest that AL may simply enhance binding and anchor E into the host membrane sufficiently to support fusion.

Our experimental results showed that in the extreme case of 100% PG, electrostatic or hydrogen bonding interactions with residues along the length of the trimer (K64, K122, K123, K202, K204, K241, K305, K307, K310, K361) are strong enough to dominate over hydrophobic interactions of the tip, and drive the trimers to a side-on orientation. However, for realistic fractions of AL, the tip-inserted conformation results. The fact that strong electrostatic or hydrogen bonding interactions lead to a side-on orientation suggests an important role for the FL in controlling the orientation. Hydrophobic interactions of the FL are important for maintaining a fusion-inducing tip-inserted orientation and avoiding an unproductive side-on orientation.

High conservation of residues in the FL among flaviviruses indicates that the FL is critical to fusion. Based on our results and prior data, we contend that the primary roles of the FL are to ensure insertion of the tip of E and to lower the energy barrier to fusion by destabilizing the target membrane [4]. Prior studies involving peptides comprised of the FL sequence have shown substantial membrane-destabilizing effects [13–15].

In a prior study of the FL of E in tick-borne encephalitus virus, Allison et al. found that mutations to L107 (within the FL) strongly impacted both binding of recombinant subviral particles to and fusion with 1:1:1:1.5 PC:PE:sphingomyelin:CHOL liposomes [23]. While the mutation L107F retained a significant degree of fusion activity, L107T impaired activity and L107D abolished fusion activity. They also showed by liposome coflotation that L107D abolished binding of recombinant subviral particles to the same liposomes. These results may seem to conflict with our conclusion that hydrogen bonding interactions of K246, K247, and R73 dominate the binding interaction over interactions of the FL, even in the absence of AL. However, replacement of L107 with the charged residue (D) will disfavor insertion of the FL into the hydrophobic core of the membrane due to the charged residue and associated water molecules. Since binding of E to CHOL-containing membranes is weak compared to AL-containing membranes, the higher energy barrier for insertion of D107 may have been sufficient to block binding.

We note that no tilt is apparent in a prior EM image of the sE trimer inserted into a 1:1:1 PC:PE:CHOL membranes [6]. However, for that case the trimer was at close-packed density where a tilted orientation may be disfavored.

In the present study, the magnitude of the tilt of membrane-bound sE was significantly lower (tilt angle ranged up to 30°) in the NR data than in the simulations (> 60°). One possible explanation is that tethering of the lipid bilayers may have substantially increased the stiffness of the membrane. Indeed, we did not observe an increase in membrane roughness upon binding, even for the case of 30% PG. Increased membrane stiffness due to tethering may produce a similar result to that observed in the fixed orientation simulations for PC:PE:CHOL. Furthermore, we also note that the experimental system involved much higher trimer coverages. This was necessary to yield a strong effect in the NR data. At such high coverages (30 vol% to 40 vol %), the trimers may be hindered from tilting to a large angle by crowding of neighboring trimers.

In a prior simulation study, the potential of mean force was determined for an E trimer as a function of distance with respect to a 70:30 PC:PG membrane [57]. In that work, the E trimer was fixed in a perpendicular orientation with respect to the membrane throughout the simulation. The minimum in free energy was found to be 15 kcal/mol. Since the present results show that sE is tilted with respect to the membrane due to increased hydrogen bonding of K246, K247, and R73 with phosphate oxygens, we conclude that the calculated value of 15 kcal/mol is a lower limit and the true free energy of interaction is substantially greater than that value. Consistent with this expectation, an experimental measurement for an 80:20 PC:PG membrane yielded a value of 20 kcal/mol [31].

Finally, we note that K246 and K247 are exposed on the surface of the mature virus and therefore may be targets for fusion inhibitors. A significant challenge in finding effective fusion inhibitors for alphaviruses and flaviviruses is that some desirable targets, such as the FL, only become accessible after the pH-dependent conformational change occurs within the endosome [45]. The fact that K246 and K247 are accessible on the surface of the mature virus outside the endosome is a feature that may be exploitable for antiviral activity. While we explored the effects of mutating residues K246 and K247 in silico, such experimental studies pose significant challenges. Structural changes that could interfere with the protein's function would need to be ruled out in order to conclude that an observed effect of the mutations on fusion is due to decreased binding affinity. While such structural studies are beyond the scope of the present work, we note that a recent high-throughput mutational study of DV serotype 3 showed that single K246 equivalent mutations (K244I and K244E in DV3) resulted in similar levels of wildtype expression, yet virions showed no detectable budding or infectivity, consistent with our proposal [8].

5. Conclusions

Residues K246, K247, and R73 form hydrogen bonds to phosphates of lipid headgroups and contribute substantially to the anchoring energy of trimeric E. These interactions contribute more enthalpic energy than hydrophobic interactions of the fusion loop. These strong hydrogen bonding interactions cause the sE trimer to adopt a tilted orientation with respect to the membrane normal and also result in increased depth of insertion. Strong interaction of the membrane with the sides of the trimer tip anchors the trimer into the membrane, while continuous contact with the FL likely destabilizes the membrane and promotes fusion of the outer leaflets. While this effect is promoted by both AL and CHOL, the effect is much greater with AL than with CHOL on a per mole basis. In agreement with prior experimental data, the simulations show that sE does not interact strongly with CHOL. CHOL facilitates hydrogen bond formation of K246 and K247 with lipid phosphate groups indirectly by increasing the distance between lipid headgroups. K246 and K247 are exposed on the surface of the mature virus and therefore may be a target for fusion inhibitors.

Transparency document

The http://dx.doi.org/10.1016/j.bbamem.2018.02.012 associated with this article can be found, in online version.

Acknowledgments

This work was supported by the Laboratory Directed Research and Development program at Sandia National Laboratories, a multi-mission laboratory managed and operated by National Technology and Engineering Solutions of Sandia, LLC., a wholly owned subsidiary of Honeywell International, Inc., for the U.S. Department of Energy's National Nuclear Security Administration under contract DE-NA-0003525. This work was also supported by NIH grant R01 AI075647 (to M.K.). This work was performed, in part, at the Center for Integrated Nanotechnologies, a U. S. Department of Energy, Office of Basic Energy Sciences user facility at Los Alamos National Laboratory (Contract DE-AC52-06NA25396) and Sandia National Laboratories. We gratefully acknowledge support from the Defense Threat Reduction Agency-Joint Science and Technology Office for Chemical and Biological Defense (IAA number DTRA10027IA-3167). We acknowledge the support of the National Institute of Standards and Technology, U.S. Department of Commerce, in providing the neutron research facilities used in this work. Research was performed in part at the National Institute of Standards and Technology (NIST) Center for Nanoscale Science and Technology. This work was supported by the NIST IMS program "Precision Measurements for Integral Membrane Proteins". This work used the Extreme Science and Engineering Discovery Environment (XSEDE), which is supported by National Science Foundation grant number OCI-1053575. Specifically, it used the Bridges system, which is supported by NSF award number ACI-1445606, at the Pittsburgh Supercomputing Center (PSC). Certain commercial materials, equipment, and instruments are identified in this work to describe the experimental procedure as completely as possible. In no case does such an identification imply a recommendation or endorsement by NIST, nor does it imply that the materials, equipment, or instrument identified are necessarily the best available for the purpose.

Appendix A. Supplementary data

Supplementary data to this article can be found online at https://doi.org/10.1016/j.bbamem.2018.02.012.

References

[1] S.C. Harrison, Viral membrane fusion, Nat. Struct. Mol. Biol. 15 (2008) 690–698.
[2] M. Kielian, Class II virus membrane fusion proteins, Virology 344 (2006) 38–47.
[3] M. Kielian, F.A. Rey, Virus membrane-fusion proteins: more than one way to make a hairpin, Nat. Rev. Microbiol. 4 (2005) 67–76.
[4] R.M. Epand, Fusion peptides and the mechanism of viral fusion, Biochim. Biophys. Acta 1614 (2003) 116–121.
[5] L. Chernomordik, M.M. Kozlov, Protein-lipid interplay in fusion and fission of biological membranes, Annu. Rev. Biochem. 72 (2003) 175–207.
[6] Y. Modis, S. Ogata, D. Clements, S.C. Harrison, Structure of the dengue virus envelope protein after membrane fusion, Nature 427 (2004) 313–319.
[7] C.Y.H. Huang, S. Butrapet, K.J. Moss, T. Childers, S.M. Erb, A.E. Calvert, S.J. Silengo, R.M. Kinney, C.D. Blair, J.T. Roehrig, The dengue virus type 2 envelope protein fusion peptide is essential for membrane fusion, Virology 396 (2010) 305–315.
[8] E.A. Christian, K.M. Kahle, K. Mattia, B.A. Puffer, J.M. Pfaff, A. Miller, C. Paes, E. Davidson, B.J. Doranz, Atomic-level functional model of dengue virus envelope protein infectivity, Proc. Natl. Acad. Sci. U. S. A. 110 (2013) 18662–18667.
[9] G. Hed, S.A. Safran, Initiation and dynamics of hemifusion in lipid bilayers, Biophys. J. 85 (2003) 381–389.
[10] L. Chernomordik, A. Chanturiya, J. Green, J. Zimmerberg, The hemifusion intermediate and its conversion to complete fusion: regulation by membrane composition, Biophys. J. 69 (1995) 922–929.
[11] J. Bentz, A. Mittal, Deployment of membrane fusion protein domains during fusion, Cell Biol. Int. 24 (2000) 819–838.
[12] M.L. Longo, A.J. Waring, D.A. Hammer, Interaction of the influenza hemagglutinin fusion peptide with lipid bilayers: area expansion and permeation, Biophys. J. 73 (1997) 1430–1439.
[13] J. Pan, C.B. Lai, W.R.P. Scott, S.K. Straus, Synthetic fusion peptides of tick-borne encephalitis virus as models for membrane fusion, Biochemist 49 (2010) 287–296.
[14] F. Stauffer, M.N. Melo, F.A. Carneiro, F.J.R. Sousa, M.A. Juliano, L. Juliano, R. Mohana-Borges, A.T. da Poian, M.A.R.B. Castanho, Interaction between dengue virus fusion peptide and lipid bilayers depends on peptide clustering, Mol. Membr. Biol. 25 (2008) 128–138.
[15] M.N. Melo, F.J.R. Sousa, Fa Carneiro, MaRB Castanho, A.P. Valente, F.C.L. Almeida, A.T. Da Poian, R. Mohana-Borges, Interaction of the dengue virus fusion peptide with membranes assessed by NMR: the essential role of the envelope protein Trp101 for membrane fusion, J. Mol. Biol. 392 (2009) 736–746.
[16] P. Larsson, P.M. Kasson, Lipid tail protrusion in simulations predicts fusogenic activity of influenza fusion peptide mutants and conformational models, PLoS Comput. Biol. 9 (2013) e1002950.
[17] D. Mirjanian, A.N. Dickey, J.H. Hoh, T.B. Woolf, M.J. Stevens, Splaying of aliphatic tails plays a central role in barrier crossing during liposome fusion, J. Phys. Chem. B 114 (2010) 11061–11068.
[18] I.A. Rodenhuis-Zybert, J. Wilschut, J.M. Smit, Dengue virus life cycle: viral and host factors modulating infectivity, Cell. Mol. Life Sci. 67 (2010) 2773–2786.
[19] E.G. Acosta, L.B. Talarico, E.B. Damonte, Cell entry of dengue virus, Futur. Virol. 3 (2008) 471–479.
[20] C. Sanchez-San Martin, C.Y. Liu, M. Kielian, Dealing with low pH: entry and exit of alphaviruses and flaviviruses, Trends Microbiol. 17 (2009) 514–521.
[21] V.C. Luca, C.A. Nelson, D.H. Fremont, Structure of the St. Louis encephalitis virus postfusion envelope trimer, J. Virol. 87 (2013) 818–828.
[22] S.J. Seligman, Constancy and diversity in the flavivirus fusion peptide, Virol. J. 5 (2008) 27.
[23] S.L. Allison, J. Schalich, K. Stiasny, C.W. Mandl, F.X. Heinz, Mutational evidence for an internal fusion peptide in flavivirus envelope protein E, J. Virol. 75 (2001) 4268–4275.
[24] A.L. Lomize, I.D. Pogozheva, M.A. Lomize, H.I. Mosberg, The role of hydrophobic interactions in positioning of peripheral proteins in membranes, BMC Struct. Biol. 7 (2007).
[25] S. Yalovsky, M. Rodriguez-Concepcion, W. Gruissem, Lipid modifications of proteins - slipping in and out of membranes, Trends Plant Sci. 4 (1999) 439–445.
[26] M.D. Resh, Trafficking and signaling by fatty-acylated and prenylated proteins, Nat. Chem. Biol. 2 (2006) 584–590.
[27] R.M. Peitzsch, S. McLaughlin, Binding of acylated peptides and fatty acids to phospholipid vesicles: pertinence to myristoylated proteins, Biochemistry 32 (1993) 10436–10443.
[28] S.W. Gollins, J.S. Porterfield, pH-dependent fusion between the flavivirus West Nile and liposomal model membranes, J. Gen. Virol. 67 (1986) 157–166.
[29] J. Corver, A. Ortiz, S.L. Allison, J. Schalich, F.X. Heinz, J. Wilschut, Membrane fusion activity of tick-borne encephalitis virus and recombinant subviral particles in a liposomal model system, Virology 269 (2000) 37–46.
[30] K. Stiasny, C. Koessl, F.X. Heinz, Involvement of lipids in different steps of the flavivirus fusion mechanism, J. Virol. 77 (2003) 7856–7862.
[31] E. La Bauve, B.C. Vernon, D. Ye, D.M. Rogers, C.M. Siegrist, B.D. Carson, S.B. Rempe, A. Zheng, M. Kielian, A.P. Shreve, M.S. Kent, Method for measuring the unbinding energy of strongly-bound membrane-associated proteins, Biochim. Biophys Acta 1858 (2016) 2753–2762.
[32] M. Umashankar, C. Sanchez-San Martin, M. Liao, B. Reilly, A. Guo, G. Taylor, M. Kielian, Differential cholesterol binding by class II fusion proteins determines membrane fusion properties, J. Virol. 82 (2008) 9245–9253.
[33] E. Zaitseva, S.-T. Yang, K. Melikov, S. Pourmal, L.V. Chernomordik, Dengue virus ensures its fusion in late endosomes using compartment-specific lipids, PLoS Pathog. 6 (2010) e1001131–e1001145.
[34] R. Budvytyte, G. Valincius, G. Niaura, V. Voiciuk, M. Mickevicius, H. Chapman, H.-Z. Goh, P. Shekhar, F. heinrich, S. Shenoy, M. Losche, D.J. Vanderah, Structure and properties of tethered bilayer lipid membranes with unsaturated anchor molecules, Langmuir 29 (2013) 8645–8656.
[35] A. Zheng, M. Umashankar, M. Kielian, In vitro and in vivo studies identify important features of dengue virus pr-E protein interactions, PLoS Pathog. 6 (2010) e1001157.
[36] B.J. Kirby, P.A. Kienzle, B.B. Maranville, N.F. Berk, J. Krycka, F. Heinrich, C.F. Majkrzak, Phase-sensitive specular neutron reflectometry for imaging the nanometer scale composition depth profile of thin-film materials, Curr. Opin. Colloid Interface Sci. 17 (2012) 44–53.
[37] A.G. Kikhney, D.I. Svergun, A practical guide to small angle X-ray scattering (SAXS) of flexible and intrinsically disordered proteins, FEBS Lett. 589 (2015) 2570–2577.
[38] F. Heinrich, M. Losche, Zooming in on disordered systems: neutron reflection studies of proteins associated with fluid membranes, Biochim. Biophys. Acta 1838 (2014) 2341–2349.
[39] J. Penfold, R. Thomas, The application of the specular reflection of neutrons to the study of surfaces and interfaces, J. Phys. Condens. Matter 2 (1990) 1369–1412.
[40] D.J. McGillivray, G. Valincius, F. Heinrich, J.W.F. Robertson, D.J. Vanderah, W. Febo-Ayala, I. Ignatjev, M. Losche, J.J. Kasianowicz, Structure and functional *Staphylococcus aureus* alpha-hemolysin channels in tethered bilayer lipid membranes, Biophys. J. 96 (2009) 1547–1553.
[41] F. Heinrich, T. Ng, D.J. Vanderah, P. Shekhar, M. Mihailescu, H. Nanda, M. Losche, A new lipid anchor for sparsely tethered bilayer lipid membranes, Langmuir 25 (2009) 4219–4229.
[42] P. Shekhar, H. Nanda, M. Losche, F. Heinrich, Continuous distribution model for the investigation of complex molecular architectures near interfaces with scattering techniques, J. Appl. Phys. 110 (2011) (102216-1–102216-12).
[43] J. Ankner, C.F. Majkrzak, Subsurface profile refinement for neutron specular reflectivity, Proceedings of SPIE 1738, 1992, pp. 260–269.
[44] F. Heinrich, H. Nanda, H.-Z. Goh, C. Bachert, M. Lösche, A.D. Linstedt, Myristoylation restricts orientation of the GRASP domain on membranes and promotes membrane tethering, J. Biol. Chem. 289 (2014) 9683–9691.
[45] D.E. Klein, J.L. Choi, S.C. Harrison, Structure of a dengue virus envelop protein late-stage fusion intermediate, J. Virol. 87 (2013) 2287–2293.
[46] M.H.M. Olsson, C.R. Søndergaard, M. Rostkowski, J.H. Jensen, PROPKA3:

consistent treatment of internal and surface residues in empirical pKa predictions, J. Chem. Theory Comput. 7 (2011) 525–537.
[47] N. Schmid, A.P. Eichenberger, A. Choutko, S. Riniker, M. Winger, A.E. Mark, W.F. van Gunsteren, Definition and testing of the GROMOS force-field versions 54A7 and 54B7, Eur. Biophys. J. 40 (2011) 843–856.
[48] S.-W. Chiu, S.A. Pandit, H.L. Scott, E. Jakobsson, An improved united atom force field for simulation of mixed lipid bilayers, J. Phys. Chem. B 113 (2009) 2748–2763.
[49] H.J.C. Berendsen, J.R. Grigera, T.P. Straatsma, The missing term in effective pair potentials, J. Phys. Chem. 91 (1987) 6269–6271.
[50] S. Pronk, S. Páll, R. Schulz, P. Larsson, P. Bjelkmar, R. Apostolov, M.R. Shirts, J.C. Smith, P.M. Kasson, D. Van Der Spoel, B. Hess, E. Lindahl, GROMACS 4.5: a high-throughput and highly parallel open source molecular simulation toolkit, Bioinformatics 29 (2013) 845–854.
[51] M. Liao, C. Sanchez-San Martin, A. Zheng, M. Kielian, In vitro reconstitution reveals key intermediate states of trimer formation by the dengue virus membrane fusion protein, J. Virol. 84 (2010) 5730–5740.
[52] W.C. Hung, M.T. Lee, F.Y. Chen, H.W. Huang, The condensing effect of cholesterol in lipid bilayers, Biophys. J. 92 (2007) 3960–3967.
[53] Y.-Q. Deng, J.-X. Dai, G.-H. Ji, T. Jiang, H.-J. Wang, H. Yang, W.-L. Tan, R. Liu, M. Yu, B.X. Ge, Q.-Y. Zhu, E.-D. Qin, Y.-J. Guo, C.-F. Qin, A broadly flavivirus cross-neutralizing monoclonal antibody that recognizes a novel epitope within the fusion loop of E protein, PLoS ONE 6 (2011) (e16059-16051–e16059-16058).
[54] L.V. Chernomordik, V.A. Frolov, E. Leikina, P. Bronk, J. Zimmerberg, The pathway of membrane fusion catalyzed by influenza hemagglutinin: restriction of lipids, hemifusion, and lipidic fusion pore formation, J. Cell Biol. 140 (1998) 1369–1382.
[55] E. Zaitseva, A. Mittal, D.E. Griffin, L. Chernomordik, Class II fusion protein of alphaviruses drives membrane fusion through the same pathway as class I proteins, J. Cell Biol. 169 (2005) 167–177.
[56] G.B. Melikyan, S.A. Brener, D.C. Ok, F.S. Cohen, Inner but not outer membrane leaflets control the transition from glycosylphosphatidylinositol-anchored influenza hemagglutinin-induced hemifusion to full fusion, J. Cell Biol. 136 (1997) 995–1005.
[57] D.M. Rogers, M.S. Kent, S.B. Rempe, Molecular basis of endosomal-membrane association for the dengue virus envelope protein, Biochim. Biophys. Acta Biomembr. 1848 (2015) 1041–1052.